

# Synoptic Features Associated with Temporally Coherent Modes of Variability of the North Pacific Jet Stream

KYLE S. GRIFFIN AND JONATHAN E. MARTIN

*Department of Atmospheric and Oceanic Sciences, University of Wisconsin–Madison, Madison, Wisconsin*

(Manuscript received 20 November 2015, in final form 16 August 2016)

## ABSTRACT

Time-extended EOF (TE-EOF) analysis is employed to examine the synoptic-scale evolution of the two leading modes of the North Pacific jet stream variability, namely, its zonal extension–retraction (TE-EOF 1) and the north–south shift of its exit region (TE-EOF 2). Use of the TE-EOF analysis enables a temporally coherent examination of the synoptic-scale evolution preceding and following peaks in each of the two leading modes that provides insight into the preferred evolutions of the North Pacific jet.

Composite analyses are constructed based upon selecting peaks in the principal component time series of both phases of each TE-EOF whose magnitude exceeded 1.5 standard deviations. Jet extension events are associated with an anomalous cyclonic circulation over the Gulf of Alaska that induces a low-level warm anomaly over western North America. Jet retractions are associated with a nearly opposite configuration characterized by an anomalous anticyclonic circulation over the Aleutians and anomalous low-level cold anomaly over western North America. Similar but lower-amplitude upper-level patterns are noted in the composites of the corresponding poleward/equatorward-shifted jet phases, with the poleward shift of the jet exit region tied to anomalously low geopotential heights over Alaska and anomalous low-level warmth over north-central North America. An equatorward shift of the exit region is tied to positive height anomalies over Alaska with downstream cold anomalies occurring in western North America. The more extreme downstream impacts that characterize TE-EOF 2 are also longer lasting (>5 days), suggesting potential utility in medium-range forecasts.

## 1. Introduction

Among the most ubiquitous structural characteristics of Earth's atmosphere are the narrow, rapidly flowing currents of air located near the tropopause, known as jet streams or jets. These synoptic features were largely unknown before and during World War II despite their original identification by Wasaburo Ooishi over Japan in 1924 (Lewis 2003). By the end of the war, however, the existence of jet streams was well established, drawing substantial amounts of research attention that quickly led to the discovery of separate subtropical (e.g., Loewe and Radok 1950; Yeh 1950; Koteswaram 1953) and polar (e.g., Namias and Clapp 1949; Palmén 1951; Newton 1954) jets.

The first comprehensive descriptions of North Pacific jet stream structure were provided by Mohri (1953). He

emphasized that the jet sat between contrasting air masses and that what often appeared to be a single jet entity was, in fact, a hybrid of the separate subtropical and polar jets. Considerable attention has subsequently been directed toward understanding the influence of external processes on the evolution of the jet. For instance, deep tropical convection, organized on the synoptic scale, can impact the jet either directly via upper-level divergent outflow (e.g., Archambault et al. 2013) or remotely through downstream baroclinic development (e.g., Kiladis and Weickmann 1992; Madden and Julian 1994; Higgins et al. 2000; Riemer and Jones 2010).

To date, the variability of the North Pacific jet and its resultant impacts on the regional and hemispheric flow patterns have been less thoroughly investigated. Schubert and Park (1991) conducted one of the first examinations of the intraseasonal variability of the North Pacific jet by performing an empirical orthogonal function (EOF) analysis on zonal wind filtered for a 20–70-day period. The leading mode of variability described a modulation of the zonal wind intensity in the core of the North Pacific jet, while the second leading mode described a modulation of

---

*Corresponding author address:* J. E. Martin, Department of Atmospheric and Oceanic Sciences, University of Wisconsin–Madison, 1225 W. Dayton Street, Madison, WI 53706.  
E-mail: jemart1@wisc.edu

the zonal extent of the jet. [Eichelberger and Hartmann \(2007\)](#) further highlighted the important role that the modulation of the jet's zonal extent plays in explaining jet variability on weekly time scales over the North Pacific. They attributed one of their analyzed modes of variability to a combination of a north–south shift, pulsing intensity, and extension–retraction of the jet stream over the North Pacific, portraying the variability of the jet on the synoptic scale to be significantly more complicated than that revealed in the analysis of [Schubert and Park \(1991\)](#).

Among the earliest studies to note the regional impacts of interannual variability of the North Pacific jet was that of [Chu et al. \(1993\)](#). They showed that differences in the zonal extent of the jet had an enormous impact on rainfall in Hawaii, as a zonally retracted (extended) jet in 1982/83 (1981/82) was associated with an extremely wet (dry) winter. [Otkin and Martin \(2004\)](#) constructed a synoptic climatology of low-frequency Kona storms near Hawaii using 10 yr of ECMWF Tropical Ocean and Global Atmosphere (TOGA) surface and upper-air data. They found that a retracted jet was associated with the increased low frequency of Kona storms in the central Pacific, suggesting that with the jet exit region retracted west of its climatological position near the date line, the waveguide was absent north of the Hawaiian Islands, consequently allowing unimpeded equatorward propagation of extratropical disturbances to the subtropics in that longitude sector.

More recently, the studies of [Athanasiadis et al. \(2010\)](#) and [Jaffe et al. \(2011\)](#) identified two leading modes of variability of the North Pacific jet. Both studies employed EOF analyses of unfiltered zonal wind data and found the leading mode consisted of a longitudinal shift of the North Pacific jet exit region such that in the extended phase (EOF 1+) the jet reached as far eastward as the west coast of North America, while in the retracted phase (EOF 1–) the jet extended only as far as 160°E. The second mode highlighted a 10°–15° meridional shift in the jet exit region (EOF 2+, a northward shift; EOF 2–, an equatorward shift). [Jaffe et al. \(2011\)](#) also investigated the synoptic evolution of sudden jet retractions and found the characteristic time scale for such events was ~10 days.

Thus, of the four characteristic North Pacific jet configurations associated with the leading two modes of variability (EOF 1+, EOF 1–, EOF 2+, and EOF 2–), only the synoptic evolution of jet retractions (EOF 1–) has been investigated. [Jaffe et al.'s \(2011\)](#) was undertaken by compositing on a single time of maximum jet retraction. Employment of such a method limits the ability of the composite to capture the temporal evolution of associated large- and synoptic-scale structures.

To enhance the degree of temporal coherency in the construction of composites, a robust method of identifying and describing the evolution of the jet stream structure is required. This paper adapts the extended EOF methodology (e.g., [Weare and Nasstrom 1982](#); [Wilks 2011](#)) to examine the synoptic evolution of temporally coherent structures characterizing the leading modes of North Pacific jet variability. A description of the time-extended EOF (TE-EOF) method, along with details of its implementation in this study, is discussed as part of a broader description of the methodology in [section 2](#). [Section 3](#) describes the jet variability on synoptic time scales within the TE-EOF framework. Time-lagged composites, constructed based on the TE-EOF analysis, highlighting synoptic features both over the North Pacific and associated with downstream impacts over North America are presented in [section 4](#). Additional time-lagged composites of anomalous deep convection are constructed via the same methodology and presented in [section 5](#). A summary and suggestions for future work are discussed in [section 6](#).

## 2. Methodology

EOF analysis is a statistical method by which the dominant modes of variability that describe a multidimensional dataset are identified (e.g., [Hannachi 2004](#); [Wilks 2011](#)). The patterns of greatest interest in an EOF analysis are those that explain the largest fraction of variability within that dataset. In the atmosphere, EOF analyses provide insight into the primary modes of variability associated with a particular atmospheric variable over a predefined spatial region and period of time. Use of EOF analyses has led to the identification and analysis of large-scale patterns in the atmosphere [e.g., the Pacific–North American (PNA) pattern, [Wallace and Gutzler 1981](#); Arctic Oscillation (AO), [Thompson and Wallace 1998](#)], although not all EOFs have a meaningful physical interpretation. Given that each mode of variability identified by an EOF analysis is defined to be statistically independent of all other modes, changes in any one mode have no correlation with changes in any other mode. In complex systems, such as the atmosphere, the asserted mathematical independence of each mode need not be mirrored in reality. The approach taken here is to apply physical insight with this statistical approach (EOF analyses) to develop understanding that neither the physics nor statistics might provide alone.

The traditional EOF analyzes a temporal sequence of spatial information to determine patterns of spatial covariability without providing any sense of how such a pattern may evolve through time. By extending the input data to include a temporal dimension, EOF analysis

can identify the time-dependent evolution of spatial patterns. This particular extended EOF (Weare and Nasstrom 1982; Wilks 2011) has been termed TE-EOF (Roundy and Schreck 2009) and describes the leading modes of spatial-temporal evolution for the analyzed data. TE-EOF incorporates temporal variability by analyzing a number of times either side of a central reference time. By doing so, temporal data are incorporated into the TE-EOF twice—once as a way to maintain the coherence of data related to the evolution of the pattern over, for instance, a 10-day window (the additional TE-EOF dimension, termed a “TE window”) and once as the time series over which to calculate the eigenmodes and to identify the patterns (or, for TE-EOFs, the temporal evolutions) associated with each mode of variability. Weare and Nasstrom (1982) introduced the concept of extended EOF analysis in the atmospheric sciences and emphasized the utility of extended EOFs that incorporate additional temporal data due to the “significant auto- and cross-correlations in time” (p. 481) associated with the similarity of atmospheric data (specifically the broad similarities shared by any two consecutive atmospheric states). Extended EOFs have been utilized to produce multivariate extended EOF analyses (calculated with multiple variables instead of multiple times), such as those used by Wheeler and Hendon (2004) to monitor the Madden-Julian oscillation, and the time-extended EOF analyses used to forecast organized modes of tropical convection by Roundy and Schreck (2009).

The TE-EOF analyses performed in this study were constructed using 31 years (1980–2010) of data from the NCEP–NCAR reanalysis (Kalnay et al. 1996) with data at 2.5° horizontal grid spacing and 6-hourly resolution. These data provide an EOF analysis of comparable quality to one constructed from an analysis with finer horizontal resolution, such as the Climate Forecast System Reanalysis (CFSR; Saha et al. 2010) but at substantially reduced cost. Zonal wind at the 250-hPa level (i.e., the jet level) was used at each analysis time throughout the winter months of November–March (NDJFM) in the 31 seasons. The chosen spatial domain of 100°E–120°W and 10°–80°N allows sufficient space around the entrance and exit regions of the North Pacific jet stream in order to fully capture the variability directly associated with each region. The TE-EOFs are performed over a TE window of 40 time steps (10 days) using zonal wind anomalies beginning at each 6-hourly time step during NDJFM. These times are buffered by 5 days at the beginning of November and the end of March to include only 10-day TE windows that fall completely within the NDJFM period. For example, the first (second) TE window in this analysis extends from 0000 UTC 1 November to 1800 UTC 10 November

(0600 UTC 1 November–0000 UTC 11 November) and is represented by the central time (referenced as D0) of 0000 UTC 6 November (0600 UTC 6 November).

In constructing the TE-EOF analyses, tests were performed to examine the sensitivity of the resulting TE-EOF 1 and TE-EOF 2 patterns to the chosen temporal and spatial constraints on the domain. Given the broad similarity of DJF and NDJFM zonal wind EOFs (not shown), and in order to reduce the calculation time, the TE-EOFs for the sensitivity tests were calculated only over the DJF period. To test temporal constraints, the TE window length was varied from 6 to 16 days, revealing only minor changes in the TE-EOF patterns. Numerous variations of the spatial domain were tested, both increasing and decreasing the extent in all directions. Expansions of the domain captured the large zonal wind variability associated with other climatological jet streams over central Asia and eastern North America, but they did not significantly impact the pattern over the North Pacific. The spatial dimensions of the domain specified above were therefore chosen to focus on variability of the North Pacific jet while excluding other remote regions of high zonal wind variability. Tests were also performed to determine the separation of the leading EOFs in accordance with the method detailed by North et al. (1982), and the first two EOFs are well separated.

The utility of the TE-EOF methodology is evident when comparing the resultant principal components (PCs) to the PCs of a traditional EOF analysis on the same data. PCs represent a measure of how well the data at a given time project back onto a given mode of variability. A time series of PCs provides a running measure of this projection and is standardized to aid interpretation. For the NDJFM months of 2009/10, Fig. 1 compares the time-extended PC (TE-PC; from a 10-day TE window) to the traditional PC (instantaneous; calculated every 6 h) and the 10-day centered running mean of the traditional PC. While the traditional PC captures more variability of the state of the North Pacific jet stream on short time scales, since this PC is constructed with data from an individual time, it is not designed to maintain temporal coherence and appears noisy at times. Smoothing the traditional PC time series over 40 points (10 days) provides values that appear similar to, but are generally of smaller magnitude than, the TE-PC values. As a result, the TE-PC better captures the full magnitude of highly anomalous events on the 10-day time scale while eliminating much of the noise from higher-frequency variability, facilitating a focus on events on the synoptic time scale. While Fig. 1 contains data only for the 2009/10 NDJFM season, similar comparisons hold across all winters since 1980/81 and suggest the TE-EOF methodology is well suited for identifying

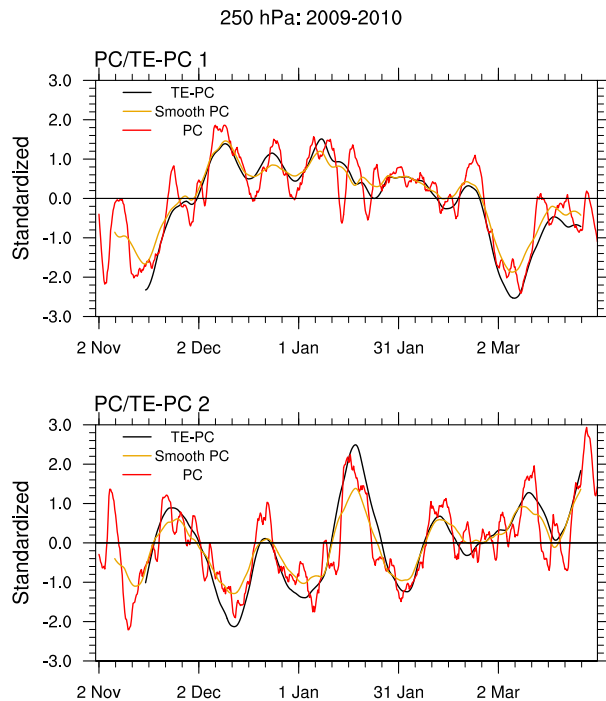


FIG. 1. Comparison of a traditional PC (red) with a 10-day smoother (brown) and a TE-PC (black) for the NDJFM 2009/10 season for the (top) leading mode and (bottom) second leading mode of variability. The standardized PCs correspond to EOFs of the 250-hPa zonal wind speed over the North Pacific.

intraseasonal shifts in the structure of the North Pacific jet stream as suggested by previous studies of North Pacific jet variability (e.g., Jaffe et al. 2011).

It is important to note that the TE-EOF modes are defined in a manner that does not require that peaks in a PC from a traditional EOF technique correspond to peaks in a mode from the TE-PC. The TE-PC captures the broader evolution of the pattern without accounting for higher-frequency signals that may project onto the traditional EOF patterns yet lack temporal longevity. It is likely these types of peaks in the PC are not captured by the TE-EOF and may account for some of the lower percent of variance explained with each TE mode when compared to the corresponding traditional EOF over the North Pacific region.<sup>1</sup> Such a reduction in explained variance by a given TE-EOF is related to the larger number of data points employed in the construction of the TE-EOF, providing increased variability for which to potentially account (Weare and Nasstrom 1982).

<sup>1</sup> The percent variance explained in Jaffe et al. (2011) for EOF 1 is 15.9%, compared to our 9.1%. Our TE-EOFs are calculated using approximately 40 times the number of data points than used in a traditional EOF analysis.

To supplement the TE-EOF analysis of the zonal wind field with physical analysis, we constructed composite analyses of high-amplitude events (those with normalized anomalous magnitudes exceeding 1.5 standard deviations) in the TE-PC time series during NDJFM for the years 1980–2010.<sup>2</sup> These composites were constructed with anomalies calculated by subtracting a 21-day centered running mean of gridded data from the NCEP–NCAR reanalysis (Kalnay et al. 1996), the same dataset used to perform the TE-EOF analyses. Such composites allow for an examination of the synoptic-scale patterns preceding and following high-amplitude peaks in given modes of jet stream variability. In addition, outgoing longwave radiation (OLR) anomalies from the NOAA interpolated OLR dataset (Liebmann and Smith 1996) were utilized in constructing additional composite analyses in order to serve as a reasonable proxy for anomalous cloud cover and convection in the tropics and subtropics. These data allow for identification of relationships between tropical/subtropical convection and the leading modes of zonal wind variability. In all composites, D0 will refer to date and time where a local maximum (or minimum) in the given TE-PC exceeded the prescribed threshold, while D – 5d and D + 5d will (as two examples) refer to the dates 5 days prior to and 5 days following D0, respectively.

### 3. Preferred modes of variability

The TE-EOF analyses presented here remain consistent with the leading modes of jet stream variability identified by previous work while explicitly incorporating the temporal evolution of synoptic time-scale patterns in the North Pacific jet stream into the analyses. Previous work has shown the spatial patterns associated with the leading modes of variability of the zonal wind over the North Pacific (e.g., Fig. 4 of Athanasiadis et al. 2010; Fig. 4 of Jaffe et al. 2011) to be similar to the patterns associated with the two leading modes of variability found at the central day (D0) of the TE-EOF analysis as shown in Fig. 2 (TE-EOF 1) and Fig. 3 (TE-EOF 2). The two other panels of Figs. 2 and 3, labeled as D – 5d and D + 5d, represent the beginning and end of the TE window, respectively. It is important to recognize that the sign associated with any EOF analysis is arbitrary and that the signs of the TE-EOFs presented here have been chosen in a manner consistent with previous literature.

<sup>2</sup> All cases within each category are well separated and so can be considered independent events.

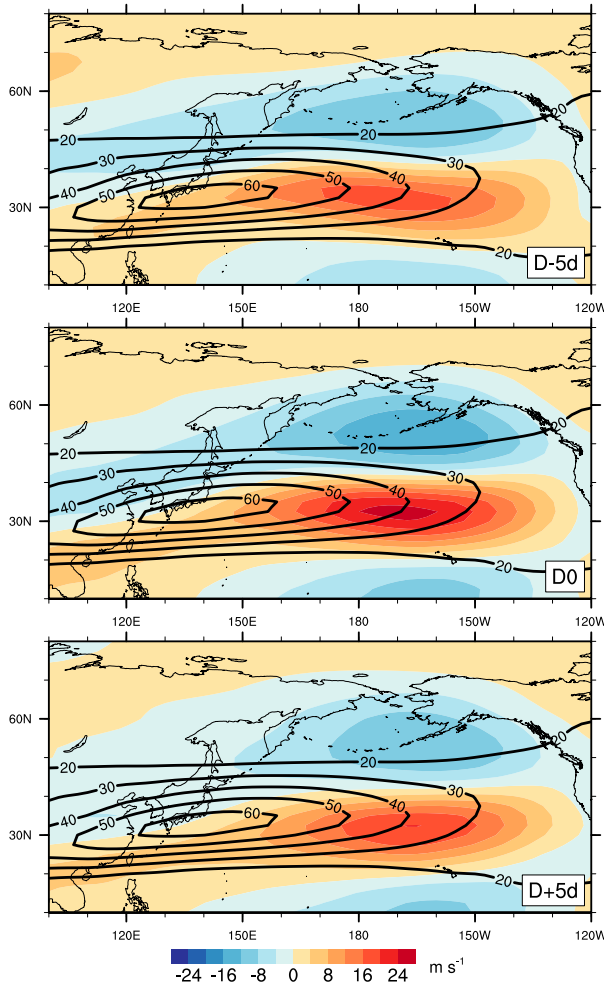


FIG. 2. TE-EOF 1 of the 250-hPa zonal wind over the North Pacific. EOF regressed back onto anomaly data is shaded ( $\text{m s}^{-1}$ ; color bar). Climatological zonal wind is contoured in black starting at  $20 \text{ m s}^{-1}$ . (top) TE-EOF pattern at the beginning of the 10-day TE window (D - 5d); (middle) the pattern halfway through the TE window (D0); and (bottom) the pattern at the end of the TE window (D + 5d).

TE-EOF 1 is composed of zonal wind variability along the latitude of the climatological jet core ( $\sim 35^\circ\text{N}$ ), with the mode's primary center of action located in the exit region of the climatological jet. Figure 2 presents the zonal wind anomalies from the NCEP-NCAR reanalysis regressed back onto the TE-EOF pattern, resulting in a maximum anomaly in excess of  $24 \text{ m s}^{-1}$  at D0 (Fig. 2b). This anomaly represents the extension (when positive) and retraction (when negative) events of the North Pacific jet characterized by TE-EOF 1. A second set of anomalies of the opposite sign can be found both poleward and equatorward of the maximum anomaly in the jet exit region. In general, the large-scale TE-EOF anomalies maximize in intensity near the central time of the 10-day TE window (D0).

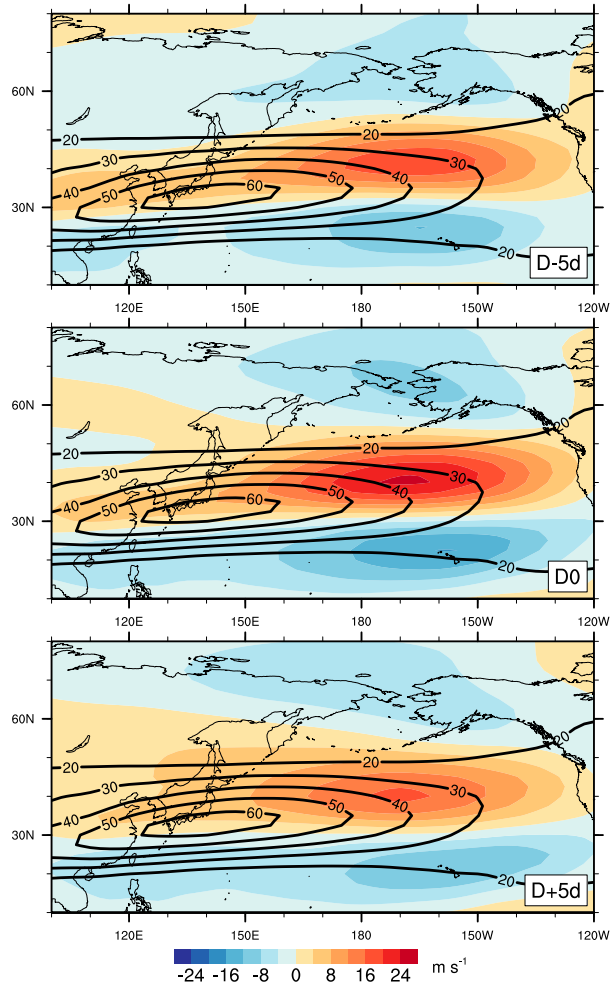


FIG. 3. As in Fig. 2, but for TE-EOF 2 of the 250-hPa zonal wind over the North Pacific.

TE-EOF 2 represents a meridional shift in the exit region of the climatological jet stream, described by a pair of anomalies of opposing sign straddling the climatological axis of the jet stream (Fig. 3). Such a pattern indicates a shift of the zonal wind to the flank of the climatological jet exit region. The northern (southern) anomaly center, when positive, represents a poleward (equatorward) shift in the jet exit region. These distinct shifts correspond to the positive and negative phases of TE-EOF 2, respectively.

#### 4. Composite analysis

To provide insight into the evolution of the synoptic-scale patterns associated with each phase of the two modes of variability, four separate composites were constructed. Each instance in which a given PC's value reached a local maxima or minima in excess of  $\pm 1.5$  standard deviations was selected for the composite.

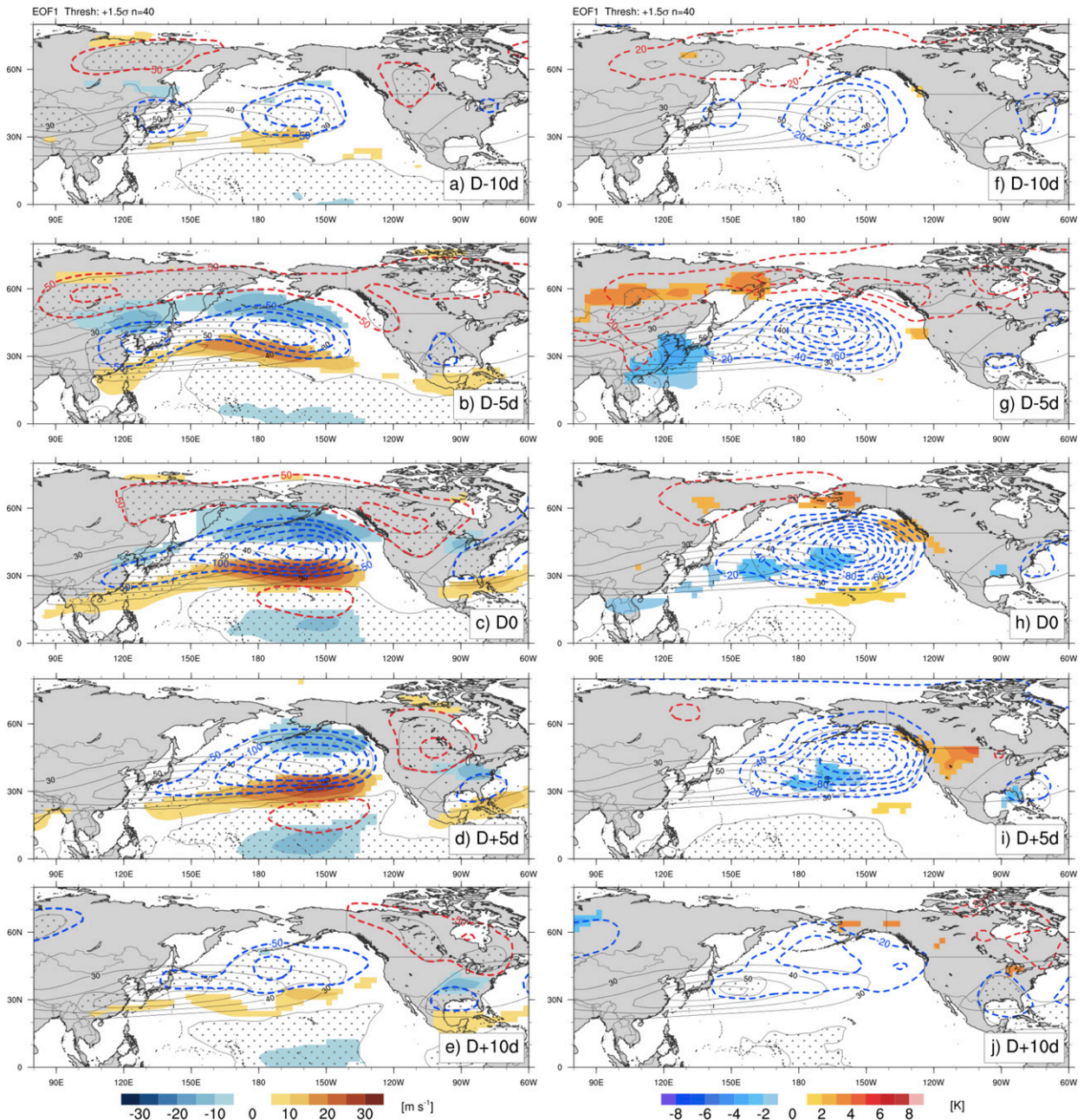


FIG. 4. Composite of cases where the PC of TE-EOF 1 was positive and  $>1.5$  standard deviations, representing jet extension cases. D0 is defined as the midpoint of the 10-day window, where  $D - 5d$  ( $D + 5d$ ) is the beginning (end) point. (a)–(e) Anomalies of 250-hPa zonal wind (shaded per color bar, only where statistically significant at 95% level) and heights (dashed contours every 50 m with blue for positive and red for negative). (f)–(j) Anomalies of 850-hPa temperature (shaded per color bar, only where statistically significant at 95% level) and heights [dashed contours as in (a)–(e), but for every 20 m]. Height anomalies in all plots are significant only within regions identified by stippling. All plots show the climatological zonal wind in thin black contours starting at  $30 \text{ m s}^{-1}$ . Composite sample size = 40.

Anomaly data from upper (250 hPa) and lower (850 hPa) levels at the selected times were averaged to produce each composite. The same NCEP–NCAR reanalysis anomaly data described in section 2 and used to originally construct the TE-EOFs were also employed in the construction of the composites.

#### a. Extension (positive TE-EOF 1)

The composite analysis of positive TE-EOF 1, created from 40 individual maxima in the PC of TE-EOF 1, is presented in Fig. 4. This positive phase represents an extension of the climatological jet over the North

Pacific with the strongest zonal wind anomaly at D0 located near 35°N, 165°W (Fig. 4c), firmly embedded within the exit region of the climatological jet. At upper levels, a negative height anomaly in the central North Pacific at D - 10d (Fig. 4a) supports a  $10 \text{ m s}^{-1}$  zonal wind anomaly on its southern flank in the exit region of the climatological jet. Strengthening to  $15 \text{ m s}^{-1}$  by D - 5d (Fig. 4b), the zonal wind anomaly extends from 150°E to 140°W while remaining equatorward of an upper-level negative height anomaly and its companion low-level anomaly (Fig. 4g) south of the Aleutian Islands. The low-level height anomaly, indicative of a cyclone, is supported at upper levels by its location in the poleward exit region of the extended jet, a region favorable for cyclone development.

Near the Asian coast at D - 10d (Fig. 4a), a separate negative height anomaly supports an enhancement of the wind speeds on the anticyclonic shear side of the climatological jet. This enhancement strengthens and zonally elongates by D - 5d (Fig. 4b), increasing upper-level flow out of the tropics near the Asian coast. Over time, this feature merges with the broader negative height anomaly in the central North Pacific (Figs. 4c,d). There, the anomalous height differential (over 300 m) between 20° and 40°N is greatest at D0 and is tied to a zonal wind anomaly of  $\sim 30 \text{ m s}^{-1}$ , effectively doubling the zonal wind in this jet exit region (Fig. 4c). The enhancement of the zonal wind in the jet exit region extends the climatological jet 20° longitude farther east, approaching the west coast of North America by D + 5d (Fig. 4d). This jet naturally follows the southern edge of the negative height anomaly in the central Pacific. Beneath the upper-level height anomaly, the 850-hPa cyclone continues to develop ( $-180\text{-m}$  minimum height anomaly) and maintains its position in the poleward exit region of the extended jet as both shift eastward (Figs. 4f-h). By D + 5d, the upper-level feature remains sprawling and moves the jet even farther east (Fig. 4d) before weakening and returning to the central North Pacific by D + 10d (Fig. 4e). Accordingly, the 850-hPa anomalous heights begin to shift onshore over western North America (Fig. 4i), indicating the low-level cyclonic anomaly is increasingly impacting the sensible weather over North America.

It is interesting to note that the height and zonal wind anomalies over eastern Asia at D - 5d, particularly those associated with the dipole of positive heights over near central Siberia and negative heights near the Korea Peninsula, weaken through D0 and are essentially absent by D + 5d. The fact that the intensity of each anomaly peaks early in the TE window suggests that this dipole may be a precursor to jet extension events over the North Pacific. This couplet is also represented in the 850-hPa

temperature anomalies, with anomalous warmth over central Siberia and anomalous cold (in excess of  $-3 \text{ K}$ ) over eastern China at D - 5d (Fig. 4g).

Downstream over North America, height anomalies start to amplify by D0, with positive height anomalies at 250 hPa over western Canada (Fig. 4c) associated with 850-hPa temperature anomalies in excess of  $2 \text{ K}$  (Fig. 4h). Farther downstream over the eastern portion of the United States and maritime Canada, negative height anomalies develop (Fig. 4c) in association with a small region of low-level cold anomalies in excess of  $-2 \text{ K}$  at D0 (Fig. 4h). The anomalously low heights over eastern North America support an enhancement of the upper jet on the anomaly's equatorward edge, resulting in a stronger subtropical jet over the southeastern United States and a pattern that resembles the positive PNA teleconnection pattern (Horel and Wallace 1981; Wallace and Gutzler 1981). While the upper-level height and low-level cold anomalies slowly slide southeastward through D + 5d, the warm anomalies intensify and expand over much of the western half of North America, peaking in excess of  $4 \text{ K}$  (Fig. 4i). This widespread warmth remains at D + 10d (Fig. 4j), but only a few small areas are statistically significant at the 95% level.

#### b. Retraction (negative TE-EOF 1)

Composites of the jet retraction cases (negative phase of TE-EOF 1) were constructed from 40 times in which the PC peaked below the  $-1.5$  standard deviation threshold (Fig. 5). While composites associated with the negative phase of TE-EOF 1 are not statistically required to be mirror opposites of the positive phase of TE-EOF 1 (due to the varying amplitudes of the cases used in the composite mean), the large-scale structures describing the two phases tend to exhibit this characteristic.

At upper levels at D - 10d (Fig. 5a), small positive height anomalies are located in the central North Pacific just north of the exit region of the climatological jet, supporting a small  $\sim 10 \text{ m s}^{-1}$  negative zonal wind anomaly in the exit region. By D - 5d (Fig. 5b), this region of anomalous heights south of the Aleutians intensifies substantially and expands along the entire northern flank of the climatological North Pacific jet. The core of the negative zonal wind anomalies is located near 180°, resulting in a retraction of the jet to west of the date line. Negative zonal wind anomalies peak at D0 in excess of  $-30 \text{ m s}^{-1}$  with these cases (Fig. 5c) in a region where the climatological wind is only  $\sim 45 \text{ m s}^{-1}$ . Centers of enhanced zonal winds exist both poleward and equatorward of the climatological jet stream with the positive zonal wind anomaly stronger on the poleward side. A modest upper-level

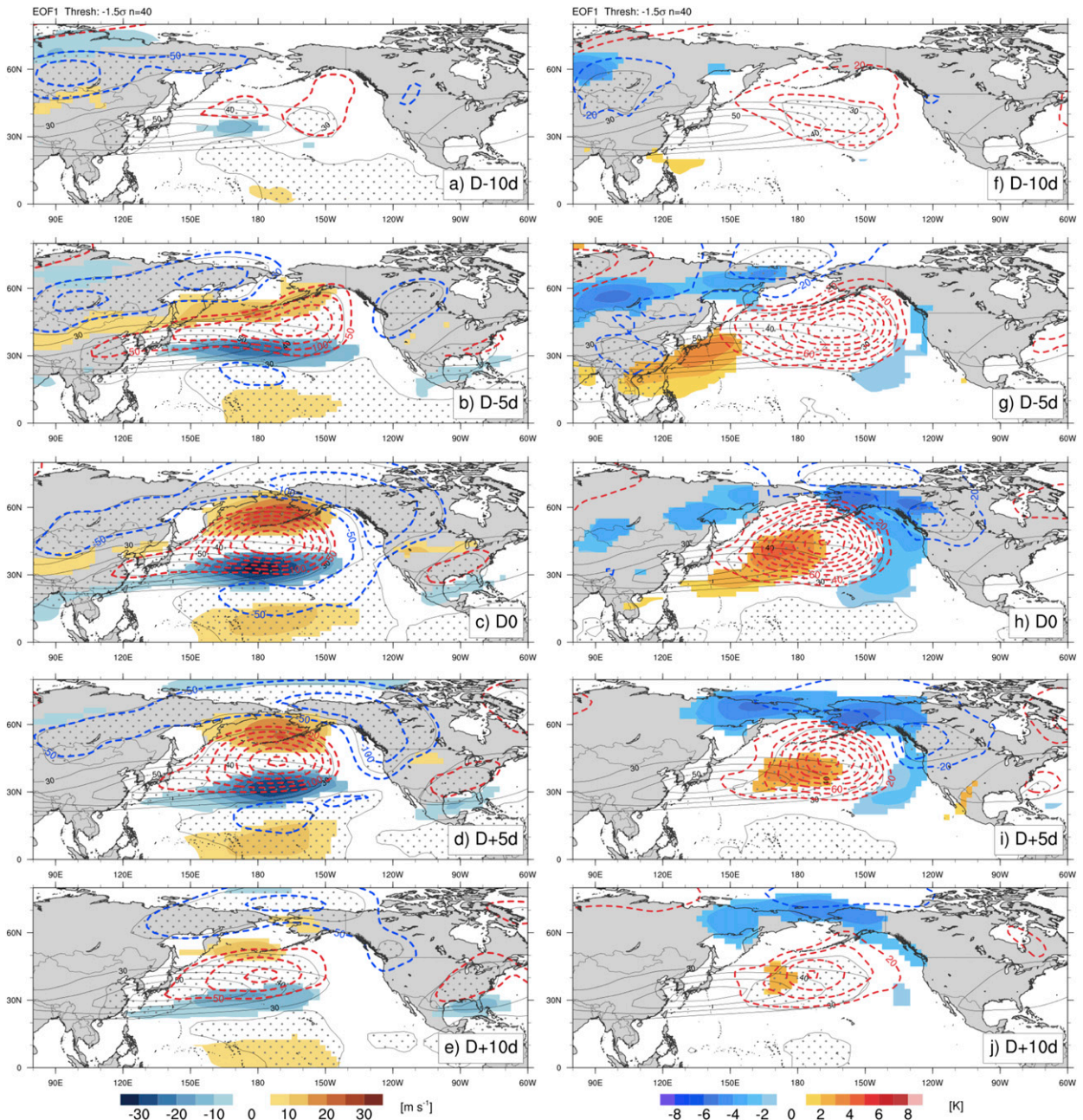


FIG. 5. As in Fig. 4, but for cases where the PC of TE-EOF 1 was  $< -1.5$  standard deviations, representing jet retraction cases. Composite sample size = 40.

negative height anomaly appears west of Hawaii at  $D - 5d$  (around  $20^{\circ}N$  and  $180^{\circ}$  longitude; Fig. 5b) and exists throughout the 10-day TE window, expanding eastward by  $D0$ . Anomalous cyclonic flow around this feature provides additional support for a reduction in climatological westerlies in the jet exit region.

East Asian precursors are comparable but roughly opposite of those of the jet extension mode (Figs. 4b,g and

5b,g). Most of Siberia is dominated by sprawling negative height anomalies at upper levels (Figs. 5a,b) and associated low-level cold anomalies (below  $-4K$ ; Figs. 5f,g), while east-central China and the Sea of Japan are dominated by a western lobe of the positive height anomaly feature that spreads eastward and consolidates with time in the 10-day TE window (Figs. 5b–d). The anomalously cold air, largely in Siberia initially (Fig. 5g), spreads

eastward to encompass Alaska and western Canada, where anomalous cold exceeds  $-5\text{ K}$  by D0 (Fig. 5h).

The downstream patterns are of similar amplitude (though of greater statistical significance) and evolve comparably to those observed in jet extension composites, but are again of reversed sign (Figs. 4d,i and 5d,i). A broad region of anomalously low heights at 850 hPa can be seen sliding out of the Arctic Ocean around D0 (Fig. 5h) and into western Canada by D + 5 (Fig. 5i), drawing cold air into Alaska for at least 10 days after peak retraction (Figs. 5h–j). While the low-level negative height anomalies over North America disappear by D + 10d (Fig. 5j), the upper-level height anomaly dipole remains significant over the central Pacific and the anomalous zonal wind magnitude remains above  $15\text{ m s}^{-1}$  beyond D + 10d.

### c. Poleward shift (positive TE-EOF 2)

Two primary centers of action straddling the mean jet exit region dominate the 10-day composite analyses of 36 poleward-shifted jet cases (cases exceeding  $+1.5$  standard deviations of TE-EOF 2). A strip of positive zonal wind anomalies north of the climatological jet axis and negative anomalies south of the climatological jet axis serves to shift that climatological jet poleward, from as far west as western China at D – 10d (Fig. 6a) to the northwestern United States beyond D0 (Figs. 6c,d). The strongest zonal wind anomalies are predominantly located poleward of the jet exit region.

A poleward shift of the jet similarly shifts the synoptic-scale height anomaly centers  $10^{\circ}$ – $15^{\circ}$  latitude poleward of the climatological jet axis. A zonally elongated positive height anomaly centered near the latitude of the climatological jet core but in the jet exit region (Fig. 6a) contrasts with a broad negative height anomaly over the Gulf of Alaska and far eastern Russia by D – 5d (Fig. 6b), helping to shift the pattern poleward and intensify the jet between the height anomalies. The negative height anomaly and its associated low-level cyclonic anomaly retrograde across the Aleutian Islands and weaken from D0 through D + 10d (Figs. 6c–e). The weakening of the negative upper-level height anomaly is coincident with an amplification of the positive height anomalies over Hudson Bay by D + 5d (Fig. 6d). While there are no significant temperature anomalies associated with the anomalous low-level cyclonic feature near the Aleutians before D – 5d (Figs. 6f,g), the anomalous tropospheric deep cyclonic flow enhances the low-level cold (warm) temperature anomalies present over the Bering Sea (central Canada; Figs. 6h–j). While the cold temperature anomalies over far eastern Russia peak in excess of  $-4\text{ K}$  at D + 5d (Fig. 6i), the corresponding warm anomalies over central Canada appear to be enhanced by

southwesterly winds downsloping off the Rocky Mountains into the Canadian Prairies and peak in excess of  $+8\text{ K}$  at D + 5d. This anomalous warmth continues to impact northeastern North America at D + 10d (Fig. 6j), although the statistically significant portion of these anomalies becomes limited.

Upstream of the North Pacific, a weak and nearly stationary region of positive height anomalies is present near the entrance region of the climatological jet at  $110^{\circ}\text{E}$  (D – 10d, Fig. 6a). This feature is maintained throughout the 20-day composite, suggesting its presence may be related to a persistent forcing such as deep convection. If so, its presence at D – 10d and D – 5d may prove to be a key precursor feature for poleward-shifted jet events.

### d. Equatorward shift (negative TE-EOF 2)

The upper-level zonal wind pattern associated with the equatorward shift mode (negative phase of TE-EOF 2) is more challenging to interpret than the composites associated with the previously discussed phases. The primary zonal wind anomalies in the composite straddle the climatological jet exit region with enhanced westerlies located on the southern periphery with a stronger region of reduced westerlies to the north prior to and throughout the 10-day window (Figs. 7a–d). This structure is similar to but opposite of the positive phase of TE-EOF 2 and is termed “equatorward shift.” While such a description allows for a convenient consistency in nomenclature, poleward-shifted jet events are not characterized by negative zonal wind anomalies in a similar location (Figs. 6b–d), providing a notable asymmetry between the positive and negative phases of TE-EOF 2. We note that the anomalous enhancement of upper-level zonal winds over Alaska and eastern Russia in this composite is of equal or greater magnitude than the enhanced westerly flow in the subtropics and may instead represent an associated invigoration of the polar jet stream (Figs. 7b–d).

The equatorward shift mode is composed of anomalous westerly zonal wind along  $20^{\circ}\text{N}$  latitude in the central Pacific throughout the composite, with the maximum westerly anomaly over the Hawaiian Islands (Figs. 7a–d). This anomalous jet extends eastward from its D – 5d position (Fig. 7b) and connects with an anomalous wind speed maximum over central North America, creating a link between the enhanced equatorward-shifted subtropical Pacific jet and the climatological jet stream over Mexico and the United States at D0 and D + 5d (Figs. 7c,d). A broad region of negative height anomalies over the western United States and central Canada acts in concert with a less

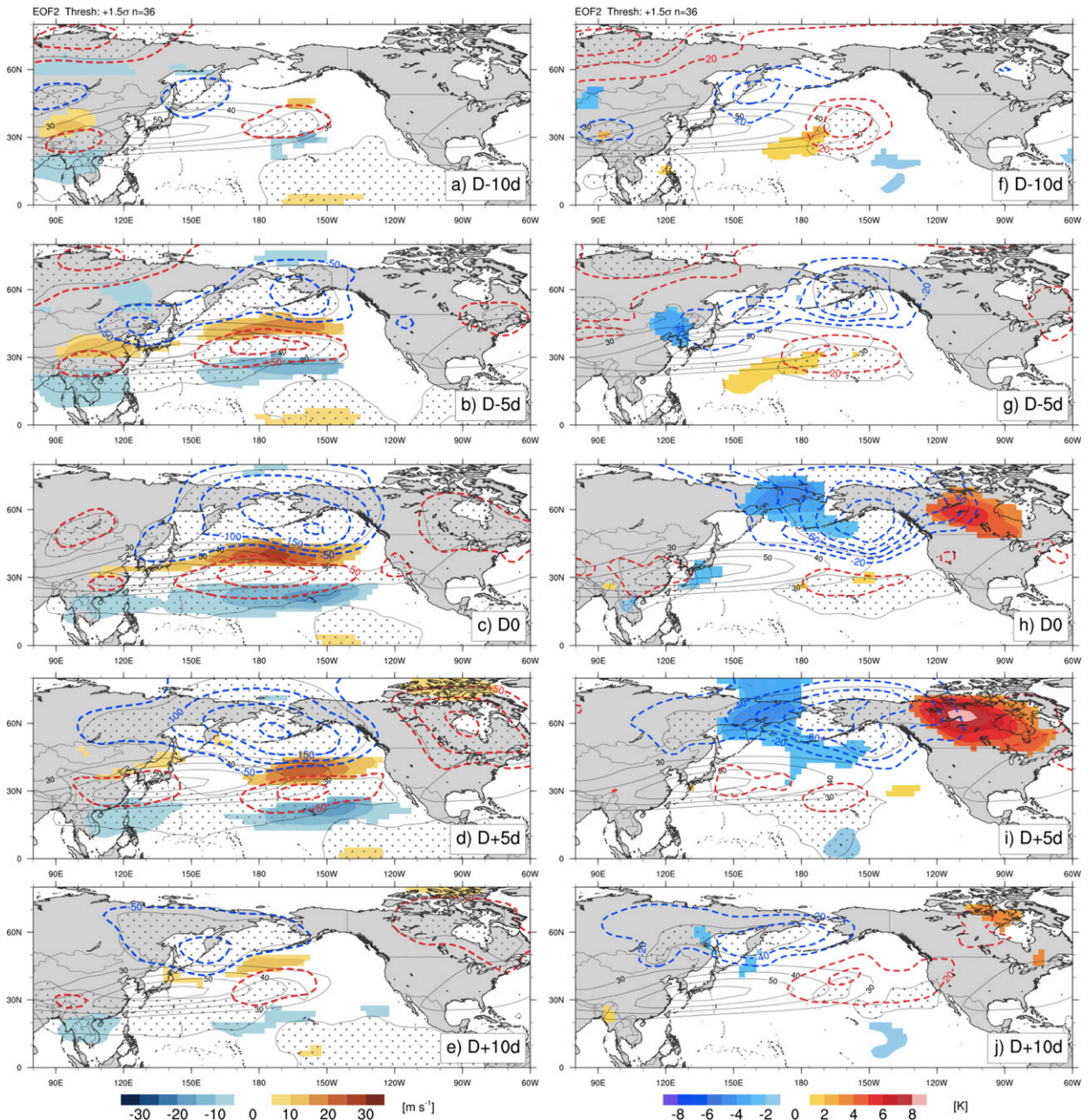


FIG. 6. As in Fig. 4, but for cases where the PC of TE-EOF 2 was  $>1.5$  standard deviations, representing poleward-shifted cases. Composite sample size = 36.

intense positive height anomaly feature in the southeastern United States to enhance the upper winds between the anomaly centers. The upper cyclonic anomaly is associated with remarkable cold anomalies in excess of  $-8$  K at 850 hPa over much of Canada (Figs. 7f–h). The magnitude of these anomalies increases dramatically as they become statistically significant between D  $-5$ d and D0 (Figs. 7f,g). Though the underlying physical mechanism driving these local

temperature tendencies is not immediately clear, some of the local temperature decrease is likely associated with cold-air advection in northwesterly low-level flow over Alaska and northwestern Canada stemming from the intensifying low-level anticyclonic anomaly over the Aleutian Islands (Figs. 7f–h).

Over the central North Pacific, a broad region of substantial upper-level positive height anomalies north of  $40^{\circ}$ N enhances the jet stream on its poleward

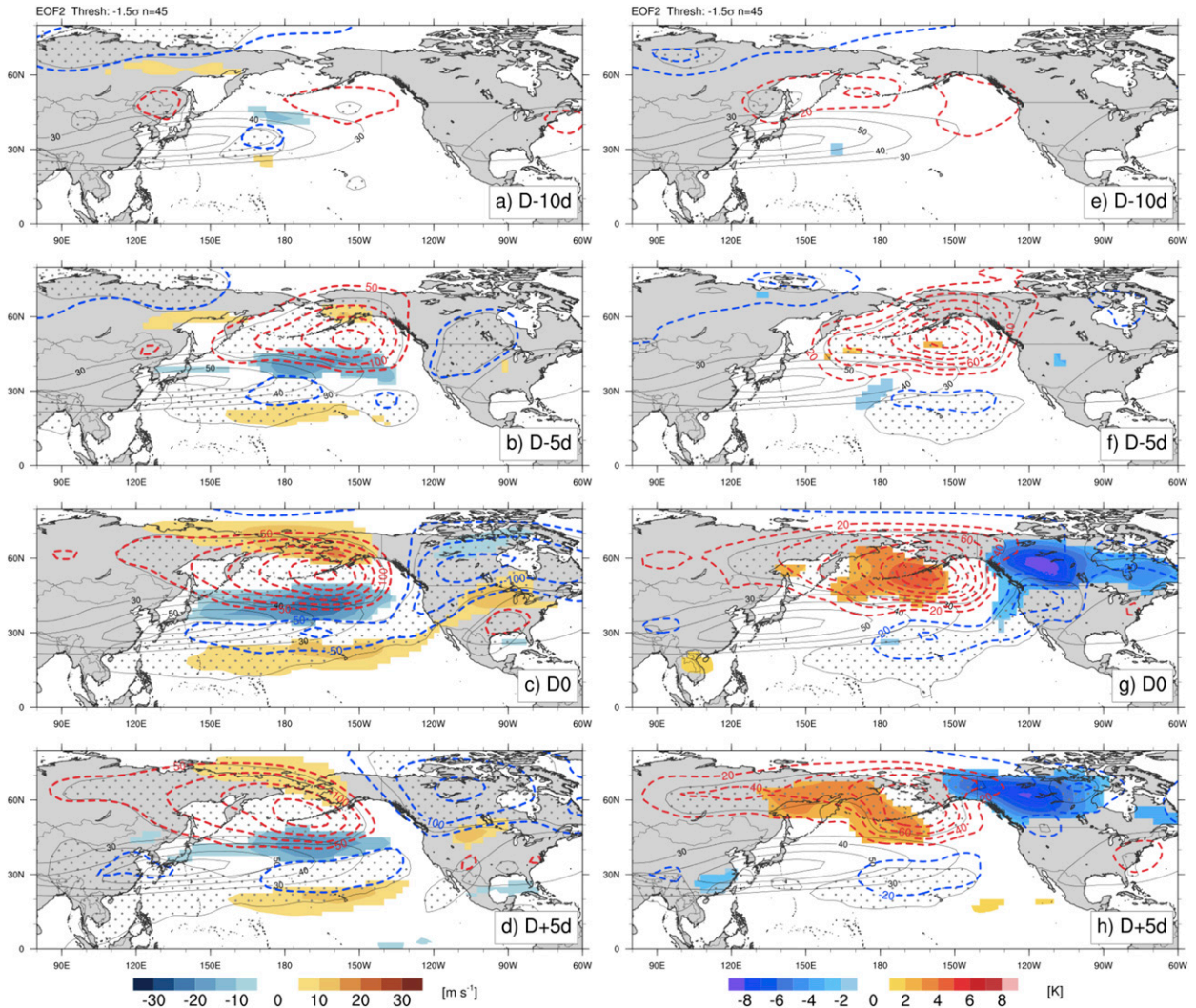


FIG. 7. As in Fig. 4, but for cases where the PC of TE-EOF 2 was  $< -1.5$  standard deviations, representing equatorward-shifted cases. Composite sample size = 45. Unlike the previous composites, D + 10d is not shown since it did not contain anomalies that appeared both physically meaningful and statistically significant.

flank, north of  $60^{\circ}\text{N}$  (Figs. 7b–d). The cross-Arctic flow associated with such a jet is also represented at the 850-hPa level and likely contributes to the anomalous low-level cold in North America at D0 and D + 5d (Figs. 7g,h). South of this upper-level feature, a broad region of anomalously low heights is present south of the climatological jet near its exit region and may represent broad upper troughs digging into the subtropics across a range of longitudes in a manner similar to that observed in jet retraction cases (e.g., Figs. 5a–e). The position suggests a connection to the Kona lows that occur in conjunction with retracted jet cases (e.g., Otkin and Martin 2004), as any such disturbance may slightly enhance the subtropical jet south of its associated trough.

The upstream patterns over Asia are diffuse with no clear-cut synoptic-scale anomalies from D – 10d to D0 at upper levels (Figs. 7b,c). This suggests that either the equatorward shift mode is triggered by well-defined but opposing synoptic-scale setups that are washed out in a composite mean analysis or that there are not any clear-cut Asian midlatitude precursors to these events.

## 5. Tropical convection composites

Although some results from the poleward-shifted jet composite suggested a connection to tropical convection, specifically the building of low-latitude anomalous ridges, such inferences are unsupported without examining proxies of the convection itself.

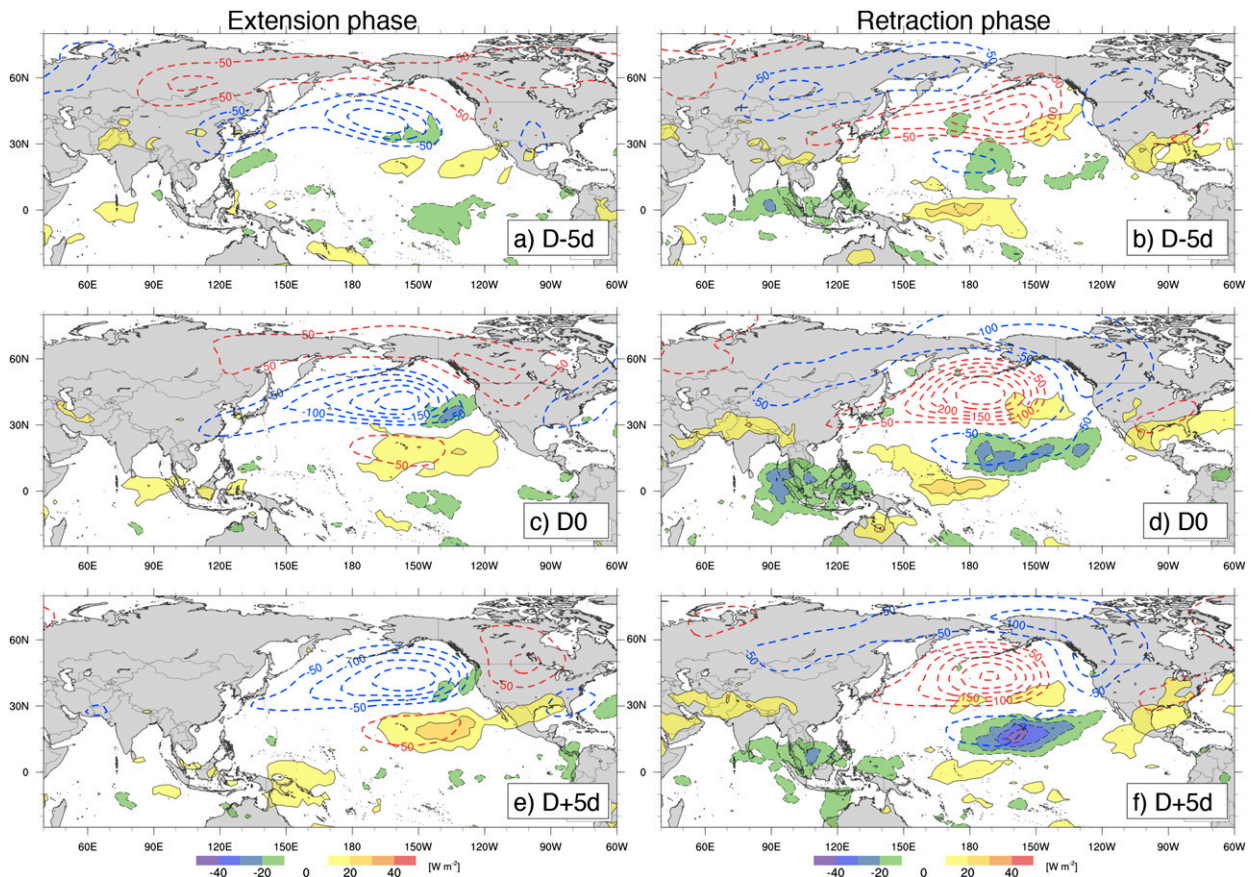


FIG. 8. Composites of OLR shaded ( $\text{W m}^{-2}$ ; color bar) calculated as in Figs. 4 and 5 for (a),(c),(e) jet extension and (b),(d),(f) jet retraction cases, respectively, from TE-EOF 1. Heights at 250-hPa contoured as in Fig. 4. Numbers of cases are consistent with the respective previous composites.

Jaffe et al. (2011) performed such composites for retracted jet cases, finding a quasi-stationary convective signal both before and after a jet retraction event. Figures 8 and 9 present OLR composites calculated as discussed in section 4 for each phase of each TE-EOF. OLR is often utilized as a proxy for cold cloud tops associated with deep convection in the tropics and subtropics, and is useful in the construction of composites due to its long, homogenous period of record. The OLR composites for the retraction mode (Figs. 8b,d,f) and the poleward shift mode (Figs. 9a,c,e) show apparent large-scale organization of anomalous enhanced tropical convection.

Anomalous tropical convection appears in the retraction composite over the eastern Indian Ocean and Maritime Continent (Figs. 8b,d,f), and it appears to move slowly eastward throughout the 10-day window of the composite. The eastward phase speed of this convection appears similar to or slightly slower than that of convection associated with the Madden-Julian oscillation (MJO; Madden and Julian 1972, Zhang 2005), which contrasts with the stationary nature of

convection found with the retraction mode in Jaffe et al. (2011). The role of this convection in fostering a retraction of the North Pacific jet is not immediately apparent. A separate region of convection in the central and eastern tropical North Pacific is consistent with the OLR composite from Jaffe et al. [2011; specifically, their day 10 composite (their Fig. 12e) and our D + 5d; Fig. 8f] near the Hawaiian Islands, although twice as intense as that found by Jaffe et al. Convection in this location is consistent with the presence of the low-latitude trough that can be inferred from the retraction composites (Figs. 5b–d). Notably, the distribution of convection prior to the mature phases of EOF 1 (Figs. 8a,b) does not correspond to that associated with the positive/negative PNA evolutions illustrated in Franzke et al. (2011, their Fig. 11).

Significant tropical convection anomalies are evident in the poleward shift composite (Figs. 9a,c,e) over Southeast Asia and the Maritime Continent and are of a larger magnitude than those observed in a similar location in association with the retraction mode. These negative

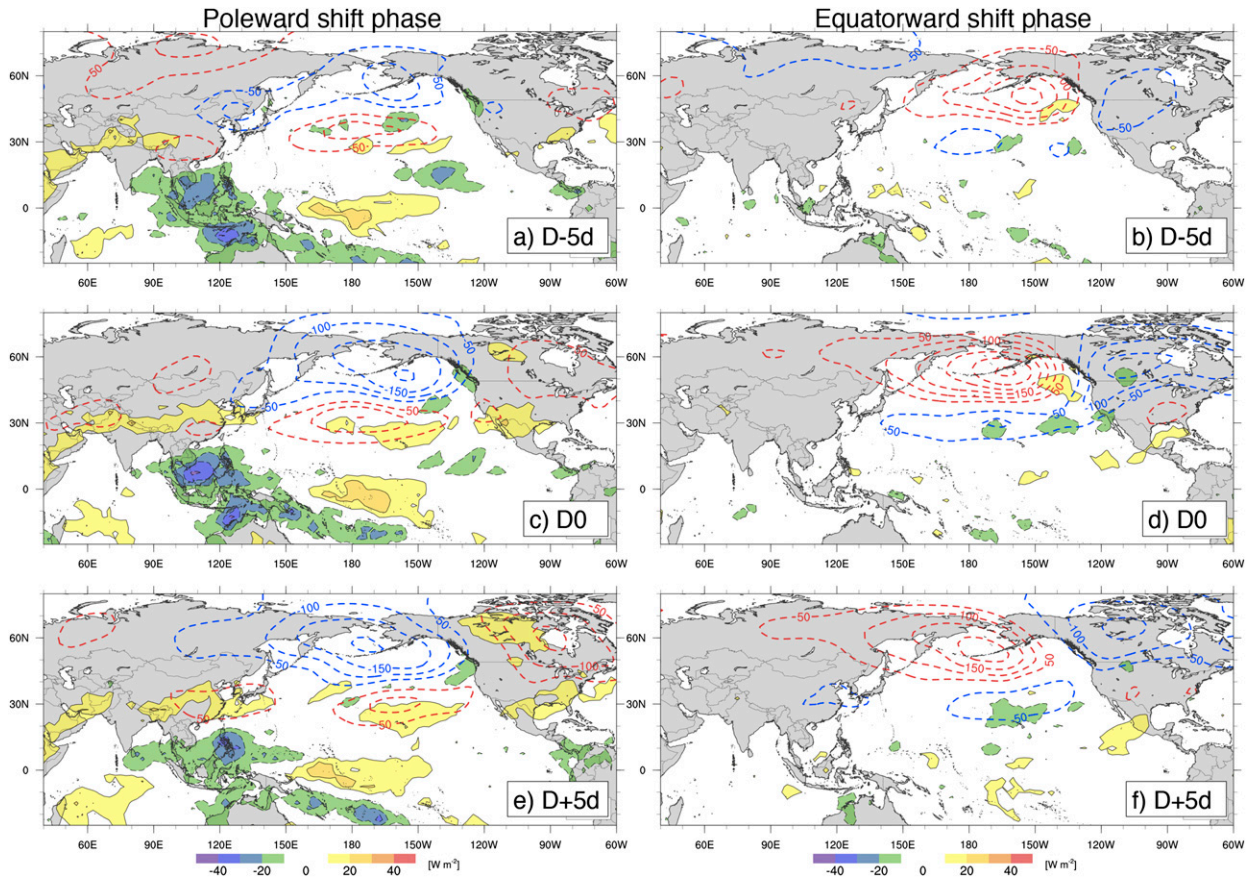


FIG. 9. As in Fig. 8, but for (a),(c),(e) poleward-shifted (from Figs. 6b–d) and (b),(d),(f) equatorward-shifted (Figs. 7f–h) jet cases from TE-EOF 2. Heights at 250 hPa contoured as in Fig. 4. Numbers of cases are consistent with the respective previous composites.

OLR anomalies also appear to remain nearly stationary or move slowly eastward, similar to convection associated with the MJO. It is interesting to note that these convective anomalies move eastward at approximately the same speed as the anomalies associated with the retracted jet events (Figs. 8b,d,f), roughly  $2^\circ \text{lon day}^{-1}$ . The quasi-stationary or slow-moving nature of these convective anomalies enables the imposition of persistent forcing on the midlatitude flow patterns that can impact both the North Pacific jet and locations downstream (e.g., Hoskins and Karoly 1981; Kiladis and Weickmann 1992; Higgins et al. 2000). Downstream impacts are commonly realized via the excitation of waves along the upper-level waveguide, or jet (e.g., Gill 1980; Simmons 1982; Martius et al. 2010), especially when the convection is located  $\sim 10^\circ\text{--}20^\circ\text{N}$  of the equator as it is in these composites' analyses. The broad low-latitude upper-level positive height anomalies in the entrance region of the poleward shift composite (Figs. 6a–e) may be a manifestation of upper-level convective outflow in this location that appears to make systematic contributions to the poleward shift of the jet.

Finally, it is worth noting that the large region of anomalously high OLR in the eastern Pacific on the equatorward side of the extended jet's exit region (Figs. 8a,c,e) is coincident with the subsiding branch of the thermally indirect circulation associated with the extended jet. This OLR anomaly intensifies throughout the 10-day composite (Figs. 8c,e). Farther north, the rising branch of the thermally indirect circulation likely enhances convection in the region of anomalously low OLR off the west coast of the United States at D0 (Fig. 8c).

## 6. Discussion

TE-EOF analysis reveals the details of the synoptic-scale evolutions associated with the leading modes of North Pacific jet stream variability. While the TE-EOF analysis presented here is consistent with the leading modes of variability previously presented by Schubert and Park (1991), Athanasiadis et al. (2010), and Jaffe et al. (2011), the TE-EOF analysis provides an additional component of temporal coherence to analyses of

the large-scale environments characteristic of extremes in the leading modes of variability, and thus points to both upstream precursors and downstream impacts.

The two primary modes of variability presented here consist of 1) the jet in either an extended or retracted state and 2) a poleward or equatorward shift of the jet exit region, respectively. While previous studies of North Pacific jet variability focused on the transition into a retracted state (Jaffe et al. 2011) and the instantaneous state of the jet in any given mode (Athanasiadis et al. 2010), the TE-EOF technique identifies the evolution of the two phases of each mode of variability centered on the peak intensity of each phase. By design, the extension/retraction and latitudinal shift modes reach their greatest extents at D0 and so employment of the TE window, which includes some of the growth of the zonal wind anomalies toward (and decay away from) such peaks, reveals new details regarding the corresponding flow evolutions.

Composites constructed based upon high-amplitude events in the TE-PC time series constitute an improvement in the temporal coherence of the associated mid-latitude signals compared to composites constructed with traditional EOFs (e.g., Jaffe et al. 2011). The development of the positive zonal wind anomalies throughout the TE window for the extended jet mode (Fig. 4) draws attention to the role of the negative height anomaly that intensifies and moves eastward throughout the following 10 days (Figs. 4a–e). This feature, suggestive of an upper trough, appears to be central to the development and intensification of the zonal wind anomalies that constitute an extended jet stream and is a central component of the synoptic evolution of the positive phase of the PNA pattern as described by Franzke et al. (2011). Expanding these composite analyses farther back in time may allow for better identification of such precursor features and their evolution over several days prior to the central time of the TE window. Forward extension of such analyses may provide additional insights into the subsequent evolution of high-amplitude events for all four phases of jet variability. The analysis suggests that, armed with a physical understanding of the precursors that drive changes in the North Pacific jet, medium-range forecasters may be better able to combine an anticipation of jet variability with the additional knowledge of the associated downstream impacts to improve large-scale forecasts into week 2 over much of North America.

Prior work by Otkin and Martin (2004) and Jaffe et al. (2011) has shown that the evolution of EOF 1 is broadly similar to the synoptic evolution of the PNA pattern. Consequently, they suggested that jet retraction and extension may be governed by some of the same physical processes as the growth of the positive–negative PNA

patterns. In their analysis of the synoptic evolution of the PNA, Franzke et al. (2011) show that convection is enhanced (weakened) over the western tropical Pacific and weakened (enhanced) over the tropical Indian Ocean, in association with the initial development of the positive (negative) PNA pattern. Such a distribution does not characterize the two phases of EOF 1 presented here. This fact suggests that the physical factors influencing the evolution of the PNA, though similar in some respects, are different in some meaningful way from those that alternately extend and retract the jet.

The composite analyses of extended jets (Fig. 4) are, at certain times, consistent with the low-level evolution of the surge phase of the East Asian winter monsoon (EAWM; Chang and Lau 1980). For instance, at D – 5d of the extended jet composite (Fig. 4g), the large area of anomalous low-level cold air over eastern China and the northern South China Sea is in a location consistent with the composite cold surge described by Chang and Lau (1980). Such cold-air outbreaks were also identified as a possible precursor to jet extension events by Jaffe et al. (2011) and may play a role in the evolution of extended jets as recently suggested by Handlos and Martin (2016).

Within these composite analyses, consistent high-amplitude impacts were noted downstream over North America in the days after the peak in the respective jet mode. For TE-EOF 1, the jet extension (retraction) mode is associated with a large region of low-level warmth<sup>3</sup> (cold) over much of Alaska and western Canada at D0 (Figs. 4h, 5h), with temperature anomalies in excess of 4 K magnitude. These anomalies suggest such weather might be a common downstream impact of each EOF 1 phase. Similarly, the phases of TE-EOF 2 are associated with even stronger downstream impacts over North America, with both poleward and equatorward shift events leading to low-level temperature anomalies in excess of 8 K. Neither of these anomalies are of high magnitude prior to D – 5d (Figs. 6g, 7f), but rather intensify over North America as the shift of the jet exit region maximizes (at D0). High-magnitude temperature anomalies are maintained through D + 5d (Figs. 6i, 7h) and up to an additional 5 days after the poleward shift (Fig. 6j), suggesting that latitudinal shifts of the jet exit region (TE-EOF 2) may affect the downstream weather over North America more significantly than jet extensions or retractions (TE-EOF 1).

<sup>3</sup>The areal extent of warm anomalies (statistically significant at the 95% level) associated with jet extensions is substantially smaller than the associated anomalies for jet retractions. However, the anomaly distributions for each species at less stringent significance levels are very similar.

A similar suggestion was made by Linkin and Nigam (2008) in their examination of the North Pacific Oscillation–west Pacific (NPO–WP) teleconnection pattern—a pattern whose upper-tropospheric geopotential and lower-tropospheric temperature anomalies are similar to those characteristic of our EOF 2. Linkin and Nigam’s study was focused solely on the mature phase structure of that mode. The details of the synoptic evolution of *both* leading modes of jet variability afforded by the TE-EOF analysis presented here provide a perspective from which a better understanding of aspects of the broader North Pacific variability—particularly determination of whether the jet is a driver of, or a response to, other fundamental aspects of that variability—might be developed.

Of the four phases associated with the two modes of variability discussed here, slow-moving and potentially organized tropical convection may play a significant role in two of them. A more complete analysis of the mid-latitude and tropical interactions that lead to these variations in the jet would serve to provide additional insight into the forcing behind such patterns, but it is beyond the scope of this study. The task of identifying such tropical–extratropical interactions has been addressed in cases of recurving tropical cyclones interacting with the jet stream (e.g., Archambault et al. 2013), but it remains a challenge for less organized episodes of persistent deep convection, which is a substantially more common phenomenon throughout the tropics and subtropics. The leading modes of jet variability broadly describe the most common evolutions of the North Pacific jet stream, implying that the most common modes of tropical convection (e.g., garden variety, as well as MJO and ENSO driven) may play a more frequent and significant role in modulating such North Pacific jet variability.

Finally, since the analyses presented here are based upon identification of the dates of *maximum* extension, retraction, and shift, the leading modes identify, for instance, the state of the jet being extended rather than the process of extension. Thus, the transitions to and from these leading modes, while partially addressed by the lagged composite analysis, merit additional study. Similarities between the jet extension and poleward shift composites (the 850-hPa Gulf of Alaska cyclonic anomaly and downstream warmth; Figs. 4, 6) and the jet retraction and equatorward shift composites (the 850-hPa Gulf of Alaska anticyclonic anomaly and downstream cold; Figs. 5, 7) suggest that the leading modes, while mathematically independent, are not physically independent. Thus, examination of the nature of transitions between the phases of each mode promises additional insight into the preferred evolutions of the North Pacific jet stream.

*Acknowledgments.* The authors thank the National Science Foundation for its support of this work via Grant AGS-1265182. OLR data were obtained from NOAA/OAR/ESRL/PSD, Boulder, Colorado, for 1979–2012 from online (at <http://www.esrl.noaa.gov/psd/>). All of the figures presented here were created using the NCAR Command Language (NCL; NCAR 2015). Finally, the suggestions of three anonymous reviewers have served to clarify the presentation of this research.

## REFERENCES

- Archambault, H. M., L. F. Bosart, D. Keyser, and J. M. Cordeira, 2013: A climatological analysis of the extratropical flow response to recurring western North Pacific tropical cyclones. *Mon. Wea. Rev.*, **141**, 2325–2346, doi:10.1175/MWR-D-12-00257.1.
- Athanasiadis, P. J., J. M. Wallace, and J. J. Wettstein, 2010: Patterns of wintertime jet stream variability and their relation to the storm tracks. *J. Atmos. Sci.*, **67**, 1361–1381, doi:10.1175/2009JAS3270.1.
- Chang, C.-P., and K. M. W. Lau, 1980: Northeasterly cold surges and near-equatorial disturbances over the winter MONEX area during December 1974. Part II: Planetary-scale aspects. *Mon. Wea. Rev.*, **108**, 298–312, doi:10.1175/1520-0493(1980)108<0298:NCSANE>2.0.CO;2.
- Chu, P., A. J. Nash, and F. Porter, 1993: Diagnostic studies of two contrasting rainfall episodes in Hawaii: Dry 1981 and wet 1982. *J. Climate*, **6**, 1457–1462, doi:10.1175/1520-0442(1993)006<1457:DSOTCR>2.0.CO;2.
- Eichelberger, S. J., and D. L. Hartmann, 2007: Zonal jet structure and the leading mode of variability. *J. Climate*, **20**, 5149–5163, doi:10.1175/JCLI4279.1.
- Franzke, C. S., S. B. Feldstein, and S. Lee, 2011: Synoptic analysis of the Pacific–North America teleconnection pattern. *Quart. J. Roy. Meteor. Soc.*, **137**, 329–346, doi:10.1002/qj.768.
- Gill, A. E., 1980: Some simple solutions for heat-induced tropical circulation. *Quart. J. Roy. Meteor. Soc.*, **106**, 447–462, doi:10.1002/qj.49710644905.
- Handlos, Z. J., and J. E. Martin, 2016: Composite analysis of large-scale environments conducive to western Pacific polar/subtropical jet superposition. *J. Climate*, **29**, 7145–7165, doi:10.1175/JCLI-D-16-0044.1.
- Hannachi, A., 2004: A primer for EOF analysis of climate data. University of Reading, 33 pp. [Available online at <http://www.met.reading.ac.uk/~han/Monitor/eofprimer.pdf>.]
- Higgins, R. W., J.-K. E. Schemm, W. Shi, and A. Leetmaa, 2000: Extreme precipitation events in the western United States related to tropical forcing. *J. Climate*, **13**, 793–820, doi:10.1175/1520-0442(2000)013<0793:EPEITW>2.0.CO;2.
- Horel, J. D., and J. M. Wallace, 1981: Planetary-scale atmospheric phenomena associated with the Southern Oscillation. *Mon. Wea. Rev.*, **109**, 813–829, doi:10.1175/1520-0493(1981)109<0813:PSAPAW>2.0.CO;2.
- Hoskins, B. J., and D. J. Karoly, 1981: The steady linear response of a spherical atmosphere to thermal and orographic forcing. *J. Atmos. Sci.*, **38**, 1179–1196, doi:10.1175/1520-0469(1981)038<1179:TSLROA>2.0.CO;2.
- Jaffe, S. C., J. E. Martin, D. J. Vimont, and D. J. Lorenz, 2011: A synoptic climatology of episodic, subseasonal retractions of the Pacific jet. *J. Climate*, **24**, 2846–2860, doi:10.1175/2010JCLI3995.1.

- Kalnay, E., and Coauthors, 1996: The NCEP/NCAR 40-Year Reanalysis Project. *Bull. Amer. Meteor. Soc.*, **77**, 437–471, doi:10.1175/1520-0477(1996)077<0437:TNYRP>2.0.CO;2.
- Kiladis, G. N., and K. M. Weickmann, 1992: Circulation anomalies associated with tropical convection during northern winter. *Mon. Wea. Rev.*, **120**, 1900–1923, doi:10.1175/1520-0493(1992)120<1900:CAAWTC>2.0.CO;2.
- Koteswaram, P., 1953: An analysis of the high tropospheric wind circulation over India in winter. *Indian J. Meteor. Geophys.*, **4**, 13–21.
- Lewis, J. M., 2003: Ooishi's observation: Viewed in the context of jet stream discovery. *Bull. Amer. Meteor. Soc.*, **84**, 357–369, doi:10.1175/BAMS-84-3-357.
- Liebmann, B., and C. A. Smith, 1996: Description of a complete (interpolated) outgoing longwave radiation dataset. *Bull. Amer. Meteor. Soc.*, **77**, 1275–1277.
- Linkin, M. E., and S. Nigam, 2008: The North Pacific Oscillation–west Pacific teleconnection pattern: Mature-phase structure and winter impacts. *J. Climate*, **21**, 1979–1997, doi:10.1175/2007JCLI2048.1.
- Loewe, F., and U. Radok, 1950: A meridional aerological cross section in the southwest Pacific. *J. Meteor.*, **7**, 58–65, doi:10.1175/1520-0469(1950)007<0058:AMACSI>2.0.CO;2.
- Madden, R. A., and P. R. Julian, 1972: Description of global-scale circulation cells in the tropics with a 40–50 day period. *J. Atmos. Sci.*, **29**, 1109–1123, doi:10.1175/1520-0469(1972)029<1109:DOGSCC>2.0.CO;2.
- , and —, 1994: Observations of the 40–50-day tropical oscillation. *Mon. Wea. Rev.*, **122**, 814–837, doi:10.1175/1520-0493(1994)122<0814:OOTDIO>2.0.CO;2.
- Martius, O., C. Schwierz, and H. C. Davies, 2010: Tropopause-level waveguides. *J. Atmos. Sci.*, **67**, 866–879, doi:10.1175/2009JAS2995.1.
- Mohri, K., 1953: On the fields of wind and temperature over Japan and adjacent waters during winter of 1950–1951. *Tellus*, **5A**, 340–358, doi:10.1111/j.2153-3490.1953.tb01066.x.
- Namias, J., and P. F. Clapp, 1949: Confluence theory of the high tropospheric jet stream. *J. Meteor.*, **6**, 330–336, doi:10.1175/1520-0469(1949)006<0330:CTOTHT>2.0.CO;2.
- NCAR, 2015: Command Language Version 6.3.0. UCAR/NCAR/CISL/TDD, doi:10.5065/D6WD3XH5.
- Newton, C. W., 1954: Frontogenesis and frontolysis as a three-dimensional process. *J. Meteor.*, **11**, 449–461, doi:10.1175/1520-0469(1954)011<0449:FAFAAT>2.0.CO;2.
- North, G. R., T. L. Bell, R. F. Cahalan, and F. J. Moeng, 1982: Sampling errors in the estimation of empirical orthogonal functions. *Mon. Wea. Rev.*, **110**, 699–706, doi:10.1175/1520-0493(1982)110<0699:SEITEO>2.0.CO;2.
- Otkin, J. A., and J. E. Martin, 2004: The large-scale modulation of subtropical cyclogenesis in the central and eastern Pacific Ocean. *Mon. Wea. Rev.*, **132**, 1813–1828, doi:10.1175/1520-0493(2004)132<1813:TLMOSC>2.0.CO;2.
- Palmén, E., 1951: The role of atmospheric disturbances in the general circulation. *Quart. J. Roy. Meteor. Soc.*, **77**, 337–354, doi:10.1002/qj.49707733302.
- Riemer, M., and S. C. Jones, 2010: The downstream impact of tropical cyclones on a developing baroclinic wave in idealized scenarios of extratropical transition. *Quart. J. Roy. Meteor. Soc.*, **136**, 617–637, doi:10.1002/qj.605.
- Roundy, P. E., and C. J. Schreck III, 2009: A combined wave-number–frequency and time-extended EOF approach for tracking the progress of modes of large-scale organized tropical convection. *Quart. J. Roy. Meteor. Soc.*, **135**, 161–173, doi:10.1002/qj.356.
- Saha, S., and Coauthors, 2010: The NCEP Climate Forecast System Reanalysis. *Bull. Amer. Meteor. Soc.*, **91**, 1015–1057, doi:10.1175/2010BAMS3001.1.
- Schubert, S. D., and C. Park, 1991: Low-frequency intraseasonal tropical–extratropical interactions. *J. Atmos. Sci.*, **48**, 629–650, doi:10.1175/1520-0469(1991)048<0629:LFITEI>2.0.CO;2.
- Simmons, A. J., 1982: The forcing of stationary wave motion by tropical diabatic heating. *Quart. J. Roy. Meteor. Soc.*, **108**, 503–534, doi:10.1002/qj.49710845703.
- Thompson, D. W. J., and J. M. Wallace, 1998: The Arctic oscillation signature in the wintertime geopotential height and temperature fields. *Geophys. Res. Lett.*, **25**, 1297–1300, doi:10.1029/98GL00950.
- Wallace, J. M., and D. S. Gutzler, 1981: Teleconnections in the geopotential height field during the Northern Hemisphere winter. *Mon. Wea. Rev.*, **109**, 784–812, doi:10.1175/1520-0493(1981)109<0784:TITGHF>2.0.CO;2.
- Weare, B. C., and J. S. Nasstrom, 1982: Examples of extended empirical orthogonal function analyses. *Mon. Wea. Rev.*, **110**, 481–485, doi:10.1175/1520-0493(1982)110<0481:EOEEOF>2.0.CO;2.
- Wheeler, M. C., and H. H. Hendon, 2004: An all-season real-time multivariate MJO index: Development of an index for monitoring and prediction. *Mon. Wea. Rev.*, **132**, 1917–1932, doi:10.1175/1520-0493(2004)132<1917:AARMMI>2.0.CO;2.
- Wilks, D. S., 2011: *Statistical Methods in the Atmospheric Sciences*. 3rd ed. Elsevier, 676 pp.
- Yeh, T., 1950: The circulation of the high troposphere over China in the winter of 1945–46. *Tellus*, **2A**, 173–183, doi:10.1111/j.2153-3490.1950.tb00329.x.
- Zhang, C., 2005: Madden-Julian Oscillation. *Rev. Geophys.*, **43**, RG2003, doi:10.1029/2004RG000158.